Investigation of inhomogeneous wave conditions in Sulafjorden

Christos Stefanakos[1], *Jian Dai*[2,3], *Bernt Leira*[2]
[1]SINTEF Ocean, Marine Modelling and Analysis, Trondheim, Norway
[2]NTNU, Marine Technology dept, Trondheim, Norway
[3]OsloMet, Civil Engineering and Energy Technology dept, Oslo, Norway

ABSTRACT

Complex fjord topography (bathymetry and coastline) may differentiate significantly wave conditions not only compared with the offshore ones but in the vicinity of few tens of meters. In the present work, possible inhomogeneities of wave conditions are investigated in a hypothetical bridge crossing in the area of Sulafjorden, central Norway. More specifically, wave conditions at ten positions across the bridge crossing have been derived by means of numerical modelling. The analysis has been carried out by transferring offshore wave conditions to the nearshore area by successive applications of the well-known third-generation wave model SWAN. As input, a very detailed bathymetry of the area, and time series of wind and wave parameters, derived from ERA5 database, have been used. At the target points, long-term time series of directional wave spectra have been used as input for the assessment of the inhomogeneity hypothesis. Various statistical features have been examined including, among others, the seasonal variability, the probability structure, the directionality, the correlation structure, and the long-term wave spectra.

KEY WORDS: significant wave height; directional spectra; floating bridge

INTRODUCTION

The study of wave conditions in an area is essential for a number of nearshore applications, such as coastal structures, marine transport, fish farming and renewable energy. Last years, the Norwegian Public Roads Administration is planning a number of large fjord crossings with different type of bridges, and the knowledge of local wave conditions is instrumental in both the design and the operational phase.

The most reliable source of information for the local wave conditions should be long-term *in situ* measurements of wave parameters. However, measurement campaigns are expensive, time consuming (since they are performed in real-time), and refer to some specific points. There is no possibility to cover large areas with buoy instruments.

On the other hand, numerical models can provide us with equally good datasets of wave parameters with some extra advantages: good spatial coverage, no gaps, reduced cost (in comparison with the measurements), easy way to update datasets (e.g., via reanalysis). Third generation spectral models (The WAMDI Group, 1988; Tolman, 1991; Booij et al., 1999) are based on a statistical representation of waves using two-dimensional (frequency-direction) wave spectra, and they are also known as phase-averaged models.

Further, the wave transformation processes of refraction, shoaling, breaking, and wind input dominate in intermediate water depths, which is within a few to tens of km from the coast. Wave heights may increase or decrease in shallower depths due to wave refraction and shoaling and wave directions refract to become more shore normal (wave crests parallel to shore). Well known models for nearshore wave transformation applications are SWAN (Booij et al., 1999), MIKE21-SW (Sørensen et al., 2004) and STWAVE (Massey et al., 2011). The input to calculate wave transformation is the output from a wave generation model (e.g., WAM) or field wave measurements, and a very precise bathymetry of the area.

Especially bathymetry plays a very important role in the transformation of wave conditions from offshore to nearshore. In the present work, possible inhomogeneities of wave conditions are investigated in a hypothetical bridge crossing in the area of Sulafjorden, central Norway. Wave conditions at ten positions across the bridge crossing have been derived by means of SWAN modelling by successive applications of the model and long-term time series of wind and wave parameters from ERA5 database as boundary conditions.

At the target points, long-term time series of directional wave spectra have been obtained and analyzed for the assessment of the inhomogeneity hypothesis. Various statistical features have been examined including the seasonal variability, the probability structure, the directionality, the correlation structure, and the long-term wave spectra. The results have been compared against the collected buoy measurements.

DATA USED

Wind and wave data from the well known climatology of ECMWF ERA5 have been used as input to the model.

ERA5 dataset, which consists of fields of wave parameters, has recently been released. Although the data cover the period 1979-2019 in hourly intervals, for the needs of the present study, the period 2010-2015 in 1-hourly intervals has been taken into account. For a more detailed description, see Hersbach et al. (2020).

In addition, and for comparison purposes, wave measurements have been used from the period 2017-2019. Measurements have been made by Fugro Oceanor, and the Meteorological Institute is responsible for data management. All measurements are stored at the Meteorological Institute, and the official data base of the Norwegian Public Roads Administration is freely available; see Met.No (2019).

The model area and the measurement data points are shown in Figure 1.

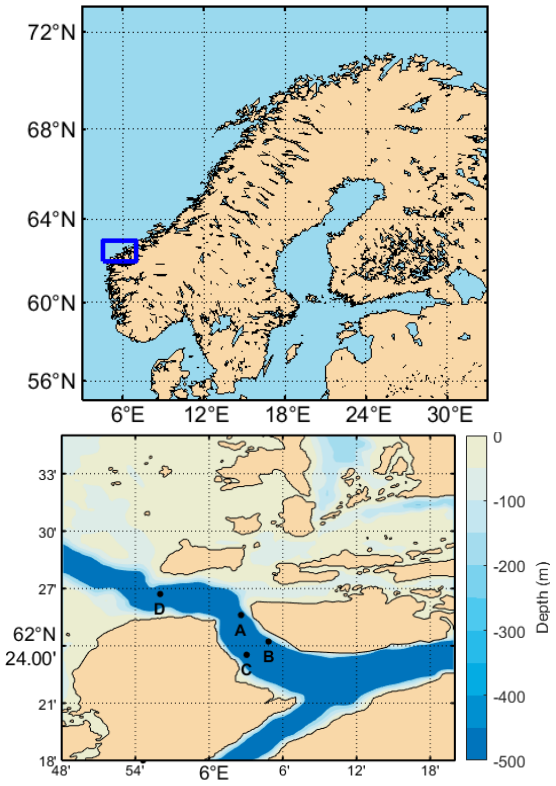

Fig. 1. Model area along and buoy positions

Finally, a very detailed bathymetry of the area (with grid step 160 m) has been used, based on the one used for our in house hydrodynamic model for ocean currents (SINMOD).

MODEL SETUP

As mentioned before, SWAN is a third-generation spectral wave model based on the evolution of the wave action density spectrum N in time, geographical, and spectral spaces, given by the action balance equation Holthuijsen (2007):

$$\frac{\partial N}{\partial t} + \frac{\partial c_x N}{\partial x} + \frac{\partial c_y N}{\partial y} + \frac{\partial c_\sigma N}{\partial \sigma} + \frac{\partial c_\theta N}{\partial \theta} = \frac{S_{\text{tot}}}{\sigma}, \tag{1}$$

where σ is the relative angular frequency, c_x, c_y are the propagation velocities of wave energy in x-, y-space, c_σ and c_θ are the propagation velocities in (spectral) σ-, θ-space. The first term of the equation represents the rate of change of action density in time, the second and third terms represent the propagation of action density in the geographic space, the fourth term represents shifting of the relative frequency due to variations in depth and currents, and the fifth term represents depth-induced and current-induced refraction.

In the right hand side, S_{tot} represents several physical processes which generate, dissipate, or redistribute wave energy. It can be described by:

$$S_{\text{tot}} = S_{\text{in}} + S_{\text{nl}} + S_{\text{ds,w}} + S_{\text{ds,b}} + S_{\text{ds,br}}, \tag{2}$$

where the right-hand side terms represent wave growth by the wind, nonlinear energy transfer, wave decay due to whitecapping, bottom friction, and depth-induced breaking, respectively.

Various parametrizations for the source terms corresponding to each physical process are available. In the present work, the wind growth formulation introduced by Yan (1987) is considered in combination with nonlinear saturation-based whitecapping (Alves and Banner, 2003; van der Westhuysen et al., 2007) (hereafter WESTH). Also, the nonlinear wave interactions are based on DIA (Hasselmann et al., 1985) and LTA methods (Eldeberky, 1996), and the bottom friction on the eddy-viscosity model (Madsen et al., 1988). The depth-induced breaking source term is modeled as

$$S_{\text{ds,br}}(\sigma,\theta) = \frac{D_{\text{tot}}}{E_{\text{tot}}} E(\sigma,\theta), \tag{3}$$

in which E_{tot} is the total wave energy and $D_{\text{tot}} < 0$ is the rate of dissipation of the total energy due to wave breaking according to Battjes and Janssen (1978).

Further, the model setup of the area is given in Figure 2 covering an area of 1 deg lat × 2.5 deg lon. The dimensions of the inner grid are 15 km × 15 km with a resolution of 150 m. The boundary points, where wave input is available, are depicted by red bullets. The in-between points of the boundary take interpolated values. In the case of land boundaries, waves are not generated, and land absorbs all incoming wave energy. Also, the runs cover the time period: 2010.01.01-2015.12.31, and the output spectra are calculated using 34 frequencies and 36 directions.

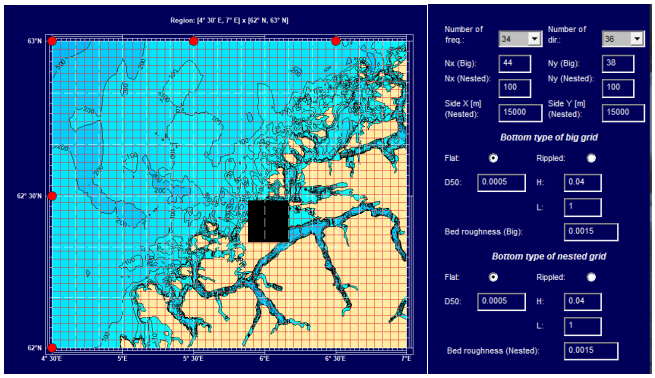

Fig. 2. Model setup (red bullets: boundary points)

NUMERICAL RESULTS

A hypothetical bridge crossing has been defined and ten points alongside have been selected for the analysis; see Fig. 3 where the points are depicted (red bullets) together with three locations (yellow triangles) where buoy measurements are available. The coordinates of all points, as well as their depths, are given in Table 1.

In addition, the distances between the 10 points are given in Table 2, where one can see that they vary according to the variations of the existing bathymetry. The distance of endpoints from the shore is: Point 1 487 m, and Point 10 491 m. The closest distance between the points of the bridge crossing and the measuring buoys is 694 m, and it is between Point 4 and buoy C.

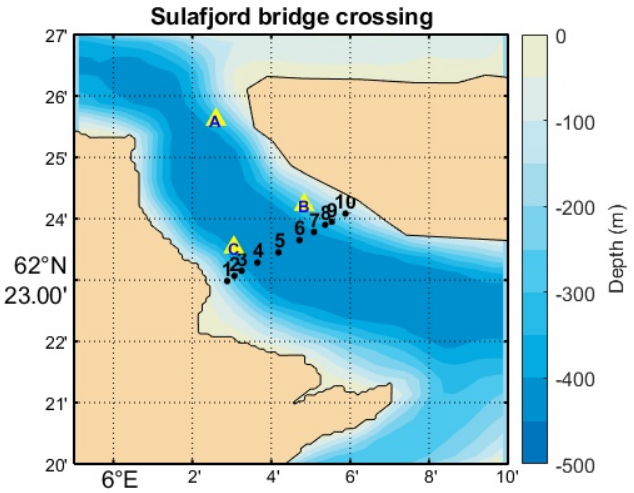

Fig. 3. Sulafjord. Red: datapoints of the bridge crossing. Yellow: measurement points

Table 1. Coordinates and depth of datapoints of the bridge crossing (numbers), and measurement points (letters)

	Longitude			Latitude			Depth
TP	deg	min	sec	deg	min	sec	m
1	6	2	53	62	22	59	234
2	6	3	4	62	23	4	329
3	6	3	15	62	23	9	368
4	6	3	39	62	23	17	419
5	6	4	11	62	23	27	441
6	6	4	43	62	23	39	436
7	6	5	5	62	23	47	403
8	6	5	22	62	23	54	350
9	6	5	32	62	23	57	304
10	6	5	53	62	24	5	161
A	6	2	36	62	25	37	284
B	6	4	50	62	24	14	262
C	6	3	3	62	23	32	404

Table 2. Distance between datapoints of the bridge crossing (in m)

Points	1-2	2-3	3-4	4-5	5-6	6-7	7-8	8-9	9-10
Distance (m)	221	221	425	554	591	402	326	171	390

Seasonal variability

Two aspects of the seasonal variability are investigated. First, the monthly variability, which is compared the corresponding one derived from the buoy measurements. For this, the monthly mean values are calculated over all available years. In Table 3 and Fig. 4, the results of this analysis are shown and compared against the measurements. The 10 points exhibit very low variability, which is comparable only with the one from buoy C.

Similarly, if one examines the daily variability of the points, one will discover that it is very low; see Fig. 5 where the daily variability of datapoint 5 is given. The thick line shows the daily mean value and the shaded area indicates the area between the min- and the max-values. Although the mean value does not exhibit significant variability, the max-values seem to show larger variability.

Table 3. Monthly mean values of the bridge crossing points (TP1-10), and measurement points (A-C)

TP	Jan	Feb	Mar	Apr	May	Jun	Jul	Aug	Sep	Oct	Nov	Dec
1	0.10	0.11	0.12	0.12	0.11	0.16	0.14	0.12	0.11	0.14	0.12	0.14
2	0.11	0.12	0.13	0.12	0.12	0.16	0.14	0.12	0.11	0.15	0.13	0.15
3	0.11	0.13	0.14	0.13	0.12	0.16	0.14	0.12	0.12	0.15	0.14	0.16
4	0.13	0.15	0.15	0.14	0.13	0.16	0.14	0.13	0.13	0.17	0.15	0.18
5	0.14	0.17	0.17	0.16	0.13	0.16	0.15	0.13	0.14	0.19	0.17	0.21
6	0.16	0.19	0.19	0.17	0.14	0.15	0.14	0.13	0.15	0.21	0.19	0.24
7	0.17	0.20	0.20	0.17	0.14	0.15	0.14	0.13	0.16	0.21	0.19	0.25
8	0.17	0.21	0.20	0.17	0.13	0.14	0.13	0.13	0.16	0.22	0.20	0.25
9	0.16	0.20	0.20	0.17	0.13	0.13	0.13	0.12	0.16	0.22	0.20	0.25
10	0.16	0.20	0.19	0.16	0.12	0.11	0.12	0.11	0.15	0.21	0.19	0.24
A	1.04	0.80	0.76	0.64	0.49	0.53	0.43	0.51	0.72	0.95	0.89	1.06
B	0.53	0.40	0.42	0.32	0.28	0.29	0.22	0.27	0.36	0.46	0.45	0.54
C	0.24	0.21	0.21	0.14	0.16	0.17	0.13	0.15	0.18	0.24	0.24	0.24

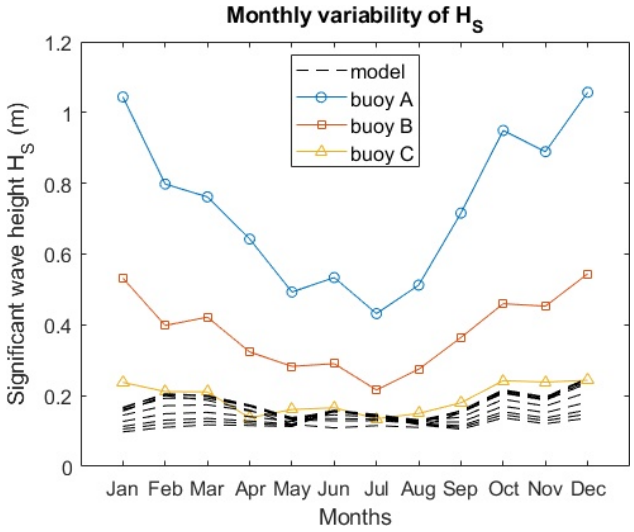

Fig. 4. Monthly variability of the bridge crossing points (dashed black lines), and measurement points (solid colored lines)

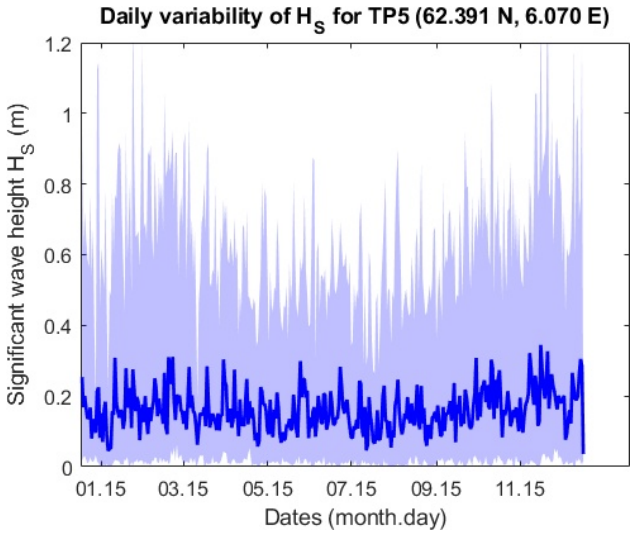

Fig. 5. Daily variability of datapoint TP5 (shaded area indicates min-max area)

Directionality

In this part of the analysis, wave roses were derived for all 10 points, as well as for the 3 measuring points (A, B, and C). The main direction is

NNW on the western side of the bridge crossing (TP1-TP4), gradually changes to NW to the eastern side (TP6-9), and becomes NWW at the endpoint (TP10).

In Fig. 6, the wave rose for TP4 is given which is compared with the closest measuring point C; see Fig. 7. The model data are in good agreement with the measurements.

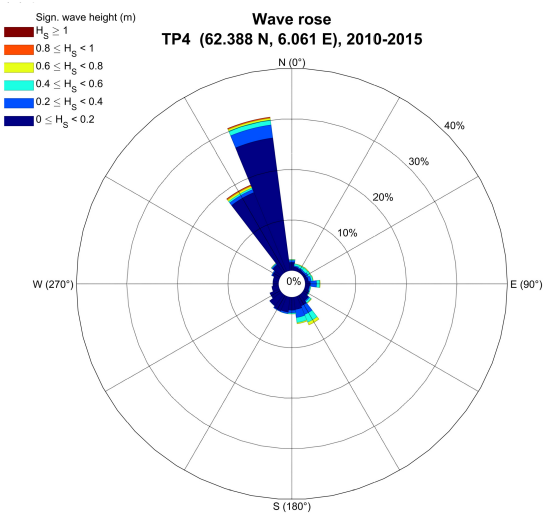

Fig. 6. Wave rose at TP4

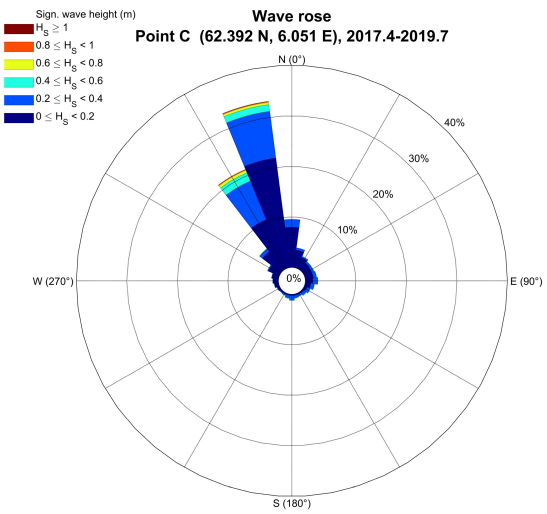

Fig. 7. Wave rose at buoy C

Probability structure

Further, the empirical probability density of significant wave height H_S and peak wave period T_p is calculated for all 10 TP points, and the 3 points with measured data. In Figs. 8~9, two examples of this analysis are given for TP4 and buoy C.

In these two figures, one can observe that probability mass related with swell is well separated from the one related with wind waves. In model data, the most probable value of swell is 0-0.1 m H_S and 9-10 s T_p with frequency of occurrence 8%, and for wind waves 0-0.1 m H_S and 2-3 s T_p with frequency of occurrence 10%. The corresponding values for buoy C are: swell, 0.1-0.2 m H_S and 9-10 s T_p (13%), and wind waves, 0.1-0.2 m H_S and 2-3 s T_p (7%).

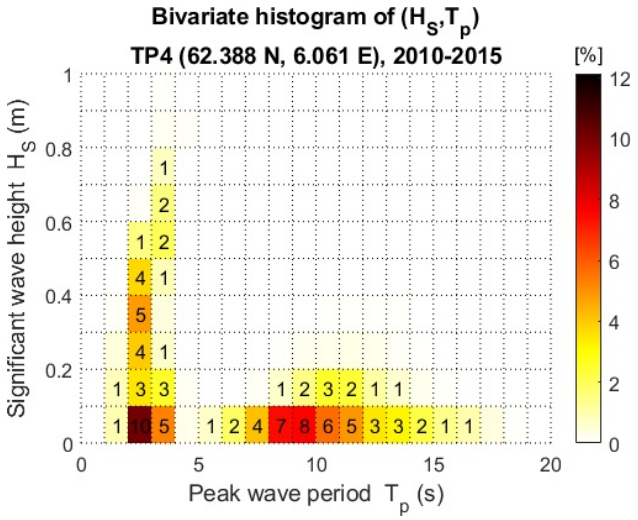

Fig. 8. Bivariate histogram of (H_S, T_p). TP4

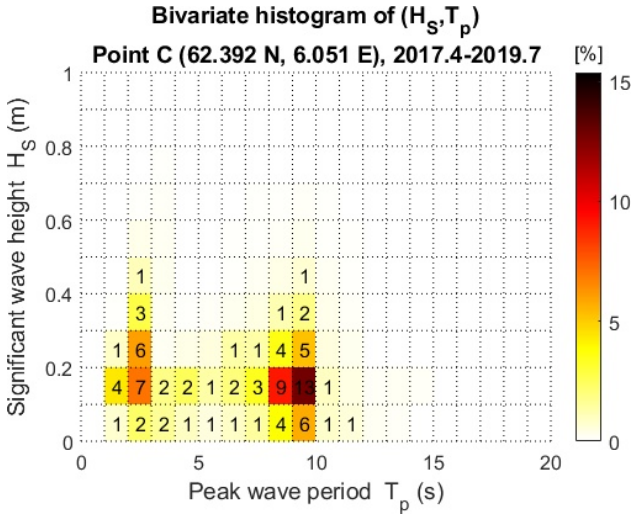

Fig. 9. Bivariate histogram of (H_S, T_p). Buoy C

Long-term wave spectra

The next step is the investigation of the long-term wave spectra. For this, long-term time series of wave spectra covering the time period 2010-2015 at a time interval of 1 hour are processed. In Fig. 10, an example of this time series is plotted for TP4. In this figure, there is an indication that at each time step swell- and wind waves-systems are well separated. This is more apparent if one plots the time series of the normalized spectra $S(f)/S(f_p)$; see Fig. 11.

Furthermore, based on the above mentioned time series, the probability structure of the frequency spectra is investigated by calculating their frequencies of occurrence (histograms). In Fig. 12, an example of these histograms is given for TP4. In this figure, one can see, for example, that the median (50%)) of the distribution varies from 10^{-5} to 10^{-3}. Also, the tail of the distribution is not very long; see, e.g., how much close are the isoprobabilities of 95% and 99% in contrast to the other end of the distribution (1% and 5%).

Finally, the probability structure is compared against results from measurements from the closest buoy C; see Fig. 3. In Fig. 13, the corresponding histogram is shown. Overall the comparison is satisfactory, considering the fact that measurements are for a different and shorter (nearly four years) time period.

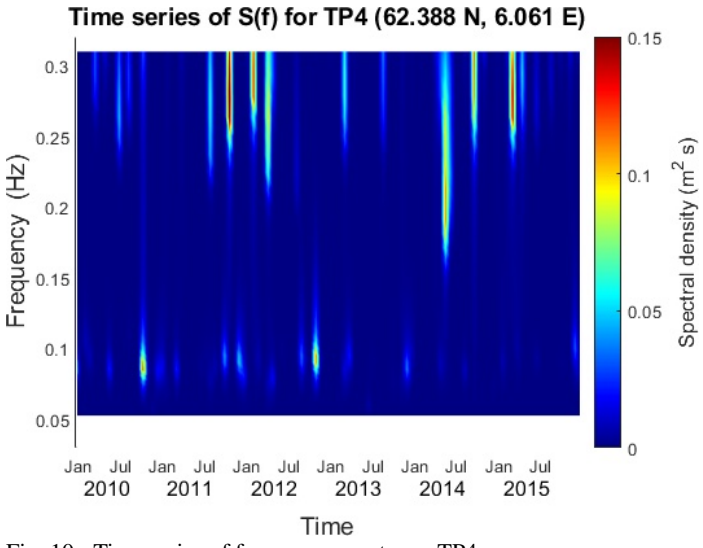

Fig. 10. Time series of frequency spectrum. TP4

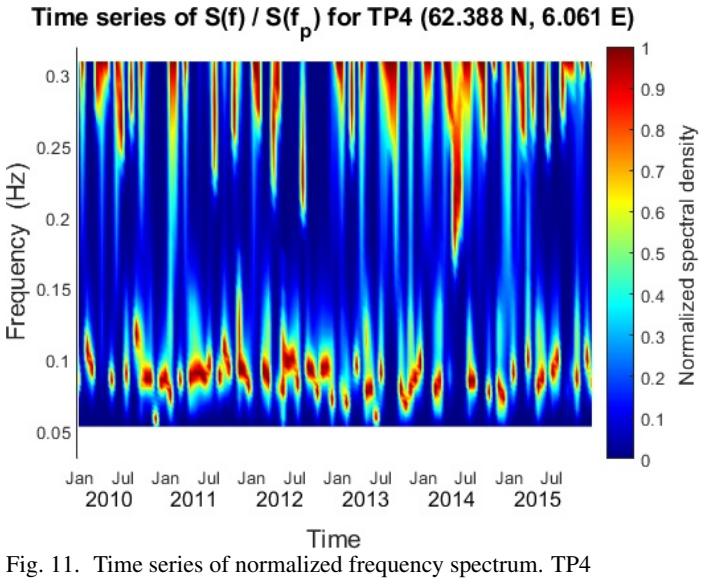

Fig. 11. Time series of normalized frequency spectrum. TP4

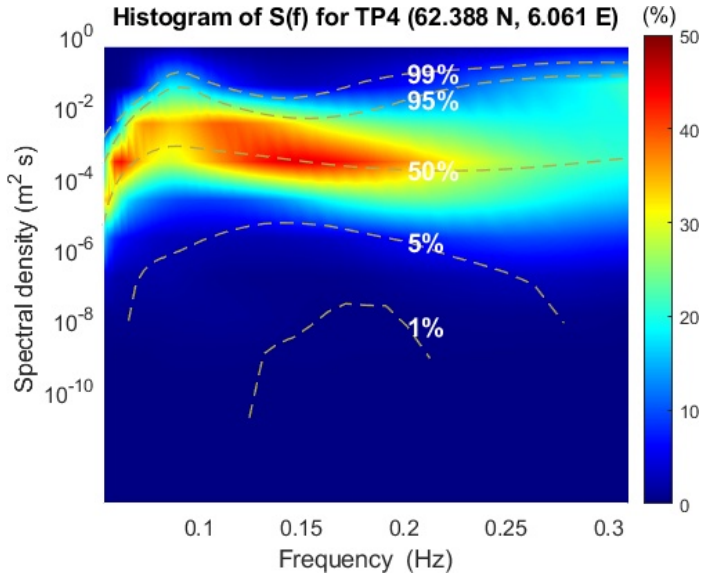

Fig. 12. Histogram of frequency spectrum. TP4

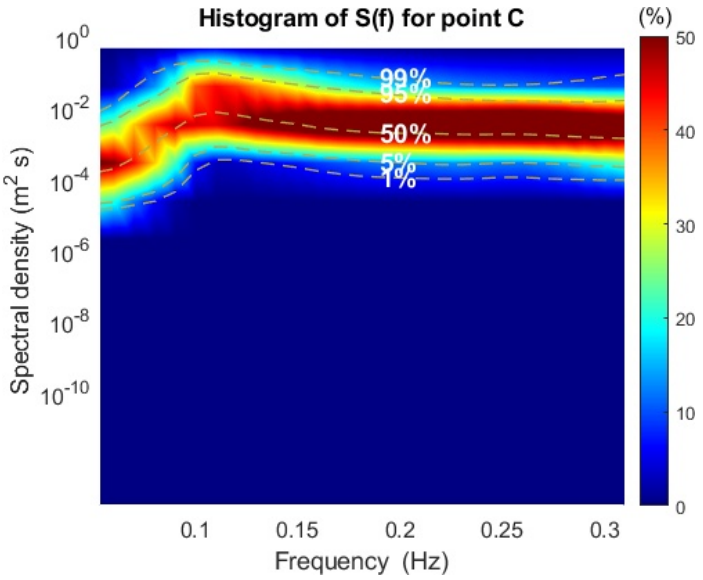

Fig. 13. Histogram of frequency spectrum. Buoy C

Correlation structure

In this section, the correlation structure of the 10 points in the bridge crossing is investigated. For this, the following Pearson's correlation coefficient R is calculated (Spanos, 1999)

$$R_{XY} \equiv R = \frac{\sum_{i=1}^{I}(X_i - \bar{X})(Y_i - \bar{Y})}{\sqrt{\sum_{i=1}^{I}(X_i - \bar{X})^2}\sqrt{\sum_{i=1}^{I}(Y_i - \bar{Y})^2}}, \tag{4}$$

where X,Y are the time series of significant wave height of any of the 10 points. The coefficient ranges from -1 to 1, where 0 means uncorrelated, 1 positively correlated, and -1 negatively correlated samples.

In Fig. 14, the matrix with the values of R for all points is plotted. In this plot, the values of the coefficient for the neighbouring points are also printed, showing strong correlation between them (98–99%). This gives the insight that for the design of the bridge, it suffices to study less points. For example, if we use only points 1,3,5,7,9, the correlation between them remains quite strong (96–98%); see Fig. 15. Even in the case, where we use only three points (1,5,9), the correlation is satisfactorily good (90–91%); see Fig. 16.

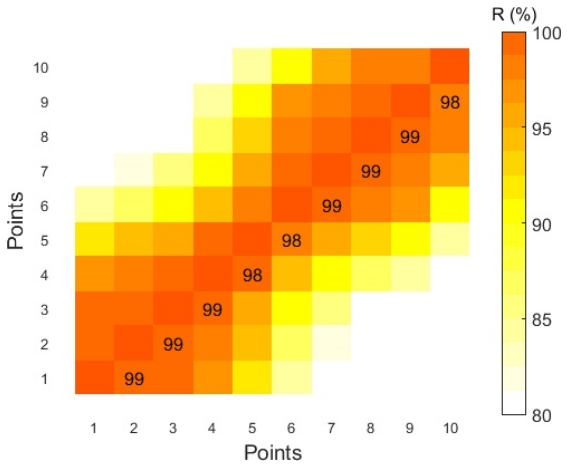

Fig. 14. Pearson's correlation coefficient R (Points: 1–10)

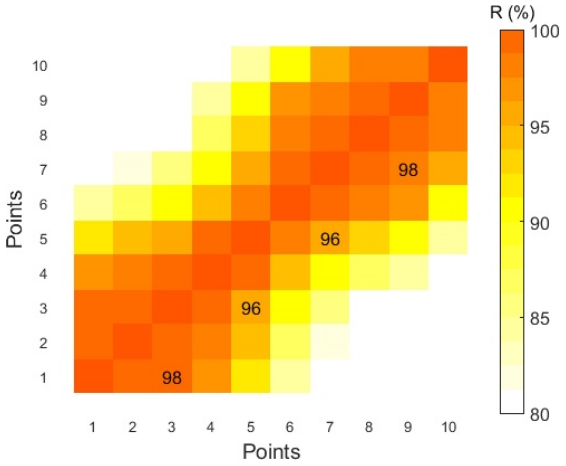

Fig. 15. Pearson's correlation coefficient *R* (Points: 1,3,5,7,9)

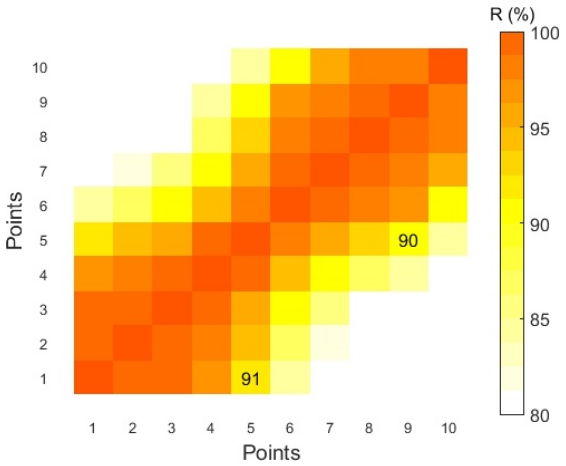

Fig. 16. Pearson's correlation coefficient *R* (Points: 1,5,9)

CONCLUDING REMARKS

In the present work, possible inhomogeneities of wave conditions are investigated in a hypothetical bridge crossing in the area of Sulafjorden, central Norway.

For this, long-term time series of directional wave spectra have been derived covering the period 2010-2015 in 1-hour intervals for ten (10) points along the hypothetical bridge crossing. Data were obtained by means of nearshore wave model SWAN, using as input offshore wind and wave conditions from ERA5 database of ECMWF and a very detailed bathymetry of the area.

Seasonal analysis of the data showed that there is no significant variability neither on monthly nor on daily basis. The existing low monthly variability is in accordance with measurements from a buoy nearby (buoy C).

Directional analysis showed that the main wave direction on the western side of the bridge crossing is NNW (TP1-TP4), gradually changes to NW to the eastern side (TP6-9), and becomes NWW at the endpoint (TP10). Again, results from model data are in good agreement with results from measurements.

The investigation of the probability structure of wave data has shown that the probability mass of swell-systems is well separated from the one related with wind waves-systems.

The study of the long-term wave spectra has given another indication that swell- and wind waves-systems are well separated.

Furthermore, the probability structure of the frequency spectra is investigated by calculating their frequencies of occurrence (histograms).

Finally, the correlation structure of the wave data is examined on the basis of Pearson's correlation coefficient, giving an insight about the possibility of using less points across the specific bridge crossing.

ACKNOWLEDGMENTS

This work was partly supported by the Research Council of Norway through the project 268403/O80 Design and Verification of Large Floating Coastal Structures - Environmental description, structural loads, responses and mooring system. We are also grateful to SVV-Midt Norge and Fugro OCEANOR AS (Lasse Lønseth) who provided the measured data via MET Norway Thredds Service at Norwegian Meteorological Institute.

REFERENCES

Alves JHGM and Banner ML (2003). "Performance of a saturation-based dissipation-rate source term in modeling the fetch-limited evolution of wind waves," *Journal of Physical Oceanography*, 33(6), 1274–1298.

Battjes J and Janssen J (1978). "Energy loss and set-up due to breaking of random waves," in *Proceedings of the 16th International Conference on Coastal Engineering*, volume I, Hamburg, Germany, pp. 569–587.

Booij N, Ris R, and Holthuijsen L (1999). "A third-generation wave model for coastal regions: 1. model description and validation," *Journal of Geophysical Research Section Oceans*, 104((C4)), 7649–7666.

Eldeberky Y (1996). *Nonlinear transformation of wave spectra in the nearshore zone*, Ph.D. thesis, Delft University of Technology, Department of Civil Engineering, The Netherlands.

Hasselmann S, Hasselmann K, Allender JH, and Barnett TP (1985). "Computations and parameterizations of the nonlinear energy transfer in a gravity-wave specturm. part ii: Parameterizations of the nonlinear energy transfer for application in wave models," *Journal of Physical Oceanography*, 15(11), 1378–1391.

Hersbach H, et al (2020). "The ERA5 global reanalysis," *Quarterly Journal of the Royal Meteorological Society*, 146(730), 1999–2049.

Holthuijsen LH (2007). *Waves in Oceanic and Coastal Waters*, Cambridge University Press.

Madsen OS, Poon YK, and Graber HC (1988). "Spectral wave attenuation by bottom friction: Theory," in *Proceedings of the 21st International Conference on Coastal Engineering*, pp. 492–504.

Massey TC, Anderson ME, Smith JM, Gomez J, and Jones R (2011). *STWAVE: Steady-State Spectral Wave Model User's Manual for STWAVE, Version 6.0*, Technical report, U.S. Army Corps of Engineers, Engineer Research and Development Center, Coastal and Hydraulics Laboratory.

Met.No. "SVV: E39 - Buoy observations," Norwegian Meteorological Institute, http://thredds.met.no/thredds/catalog/obs/buoy-svv-e39/, [accessed 2019.01].

Sørensen O, Kofoed-Hansen H, Rugbjerg M, and Sørensen L (2004). "A third generation spectral wave model using an unstructured finite volume technique," in *Proceedings of the 29th International Conference of Coastal Engineering*, Lisbon, Portugal, pp. 894–906.

Spanos A (1999). *Probability Theory and Statistical Inference*, Cambridge University Press, Cambridge.

Tolman H (1991). “A third-generation model for wind waves on slowly varying, unsteady, and inhomogeneous depths and currents,” *Journal of Physical Oceanography*, 21, 782–797.

The WAMDI Group (1988). “The WAM model-A third generation ocean wave prediction model,” *Journal of Physical Oceanography*, 18(12), 1775–1810.

van der Westhuysen AJ, Zijlema M, and Battjes JA (2007). “Nonlinear saturation-based whitecapping dissipation in SWAN for deep and shallow water,” *Coastal Engineering*, 54(2), 151 – 170.

Yan L (1987). *An improved wind input source term for third generation ocean wave modelling*, Technical Report WR-nr. 87-8, KNMI, De Bilt.